Metallopolymerization as a Strategy to Translate Ligand-Modulated Chemoselectivity to Porous Catalysts

Wen-Yang Gao,[a] Andrew A. Ezazi,[a] Chen-Hao Wang,[a] Jisue Moon,[b,c] Carter Abney,[b] Joshua Wright,[d] and David C. Powers[a,*]

[a]Texas A&M University, Department of Chemistry, College Station TX 77843, United States
[b]Chemical Sciences Division, Oak Ridge National Laboratory, P.O. Box 2008, Oak Ridge, Tennessee 37831, United States
[c]Department of Chemical Engineering and Materials Science, University of California–Irvine, 916 Engineering Tower, Irvine, CA 92697, United States
[d]Illinois Institute of Technology, 3300 South Federal Street, Chicago, Illinois 60616, United States

Abstract Porous catalysts have garnered substantial interest as potential platforms for group-transfer catalysis due to the ability to site-isolate catalysts and to non-covalently co-localize substrates in proximity to reactive intermediates. In contrast to soluble molecular catalysts, the limited synthetic toolbox available to prepare porous catalysts presents a formidable challenge to controlling the primary coordination sphere of lattice-confined catalysts and thus modulating the electronic structures of reactive catalyst intermediates. Here, we utilize Sonogashira cross-coupling chemistry to prepare a family of porous metallopolymers, in which the primary coordination sphere of Ru_2 sites is systematically varied. The newly synthesized materials are characterized by IR, elemental analysis, gas sorption, powder X-ray diffraction, thermogravimetric analysis, X-ray absorption spectroscopy, and diffuse-reflectance UV-vis-NIR spectroscopy. The resulting porous materials are catalysts for nitrene-transfer chemistry and the chemoselectivty for allylic amination of olefin aziridination can be tuned by modulating the primary coordination sphere of the catalyst sites. The demonstration of metallopolymerization as a rational synthetic strategy allows to translate ligand-modulated chemoselectivity to porous catalysts, which represents a new opportunity to tailor the functionality of heterogeneous analogues of molecular complexes.

Introduction Synthesis of crystalline metal-organic frameworks (MOFs) is predicated on reversible metal–ligand (M–L) bond-forming chemistry which simultaneously assembles the porous network and establishes the primary coordination sphere of the lattice-confined transition metal ions.[1] The necessity for reversible M–L bond formation to achieving material crystallinity limits the diversity of ligands that can be utilized to generate potential catalyst MOFs. Pyridyl-, carboxylate-, and azolate-derived ligands — all of which are fairly weak-field ligands with low-pKa conjugate acids — are ubiquitous in the chemistry of MOFs. In contrast, strongly basic donors, such as amido, amidinate, and alkoxide ligands — common ligands in molecular transition metal catalysts — are rarely, if ever, encountered in the coordination chemistry of MOFs (Figure 1a).[2, 3] In addition, because the traditional synthetic logic of MOF chemistry is based on retrosynthetic

disconnection of the M–L bonds, completely new synthetic conditions are required each time a new primary coordination sphere is sought.[4-7]

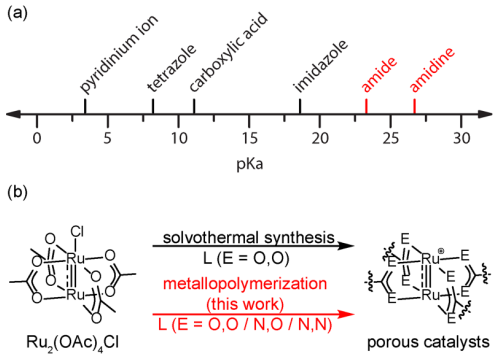

Figure 1. (a) The pKa values (in DMSO) of a series of selective functional groups coordinating with metal ions through deprotonation are summarized here (the pKa values of carboxylic acid, amide, and amidine refer to that of benzoic acid and benzamide, and benzamidine, respectively). (b) There is only one case of porous MOFs generated by solvothermal synthesis based on dimeric Ru. This work demonstrates metallopolymerization as a synthetic strategy that allows to prepare a family of porous catalysts based on Ru_2 and to atomistically control its primary coordination sphere from a wide array of ligand scaffolds.

Porous organic materials,[8, 9] such as crystalline covalent-organic frameworks (COFs),[10-12] amorphous porous organic polymers (POPs),[13-17] and organic cage compounds[18, 19] are comprised of exclusively organic components connected via covalent bonds. A diverse set of reactions, including imine and boronic ester condensations,[20, 21] nitrile cyclotrimerizations,[22] nucleophilic aromatic substitutions,[23] C–C and C–N cross-coupling reactions,[24-26] and Huisgen cycloadditions[27] have been applied to the synthesis of porous organic materials. We were attracted to the potential to utilize the polymerization strategies pioneered in POPs, in combination with pre-formed metallomonomers containing the specific metal coordination site of interest, to generate new porous materials in which the primary coordination sphere of site-isolated catalysts could be systematically tuned. Because the envisioned synthetic logic is based on retrosynthetic disconnection of covalent bonds within the organic linkers, and not on the M–L bonds, we speculated that this synthetic approach would 1) provide access to families of catalyst materials in which the primary coordination sphere of the catalyst sites could be systematically tuned, and 2) would enable the synthesis of these materials[28, 29] via a common synthetic protocol.

The ability to utilize systematic ligand perturbation to control the chemoselectivity of substrate functionalization reactions is a hallmark of molecular catalyst design. For example, the selection between allylic C–H amination and aziridination products during Ru_2-catalyzed nitrene-transfer reactions intimately depends on the primary ligand set that supports the Ru_2 catalyst.[30] Porous metal-organic frameworks (MOFs), comprised of metal nodes and organic linking elements, have been advanced as platforms to achieve intermolecular group-transfer catalysis by non-covalently co-localizing substrates in proximity to lattice-bound reactive intermediates.[31-33] In contrast to soluble molecular catalysts, in which the primary coordination sphere can be easily modified, efforts to

evaluate the potential of MOF catalysts as platforms for chemoselective group transfer catalysis, such as C–H amination, are hampered by the current inability to rationally control the primary coordination sphere of catalyst sites, and thus the electronic structure of catalyst-supported reactive intermediates, confined within the extended lattice of porous catalyst materials.

Here we report the synthesis of a family of porous polymer materials featuring Ru_2 sites supported by a diverse family of bridging ligands, including carboxylate, amidate, 2-hydroxypyridinate, and 2-aminopyridinate. The materials are readily accessed by Sonogashira cross-coupling chemistry between preformed molecular Ru_2 monomers decorated with aryl iodide functionality and polyalkynes. Consistent with the irreversible Sonogashira reactions utilized to generate these materials,[34] the new Ru_2-based porous polymers are amorphous. These new porous materials are competent nitrene transfer catalysts in both intra- and intermolecular C–H amination. Importantly, in the context of intramolecular nitrene transfer in olefinic substrates, the selectivity for allylic amination and olefin aziridination displays ligand-dependent selectivity that mirrors analogous soluble molecular catalysts. We anticipate that the synthetic strategy described herein, which provides access to porous materials that combine the site isolation of catalyst sites characteristic of MOF chemistry with the atomistic control over the primary coordination sphere of transition metal ions that is central to controlling catalyst activity in molecular catalysis, will provide new opportunities to develop porous catalysts for chemoselective group-transfer chemistry.

Results

Synthesis of molecular complexes. A family of molecular Ru_2[II,III] complexes bearing iodinated bridging ligands were prepared by thermally promoted ligand exchange with $Ru_2(OAc)_4Cl$ (Figure 2). Exchange reactions were carried out with 4-iodobenzoic acid (4-I-HOBz), 4-iodobenzamide (4-I-H_2NBz), 2-hydroxy-4-iodopyridine (4-I-hp), 2-hydroxy-5-iodopyridine (5-I-hp), and 2-amino-4-iodopyridine (4-I-ap), to provide Ru_2(4-I-OBz)$_4$Cl, Ru_2(4-I-HNBz)$_4$Cl, Ru_2(4-I-hp)$_4$Cl, Ru_2(5-I-hp)$_4$Cl, and Ru_2(4-I-ap)$_4$Cl, respectively. In each case, ligand substitution reactions were followed by electrospray ionization mass spectrometry (ESI-MS; negative mode), which provided a value of m/z that corresponded to the mass of $[Ru_2L_4Cl_2]^-$. Structurally, these Ru_2[II,III] complexes are comprised of a binuclear core supported by four bridging ligands; charge balance of the Ru_2[II,III] mixed-valent core is achieved with an axially bound chloride ligand (see, for example, the structure of Ru_2(4-I-HNBz)$_4$Cl derived from single-crystal X-ray diffraction, Figure S1 and Table S1). The electronic absorption spectrum of the iodinated Ru_2 complexes are well-matched to the spectral data for non-iodinated analogues (Figure S2). In addition, the ^{1}H NMR spectrum of Ru_2(4-I-OBz)$_4$Cl (Figure S3) displays similar paramagnetically shifted signals as $Ru_2(OBz)_4Cl$.[31] Ru_2(4-I-hp)$_4$Cl, Ru_2(5-I-hp)$_4$Cl, and Ru_2(4-I-ap)$_4$Cl do not display ^{1}H NMR signals when measured in DMSO at 295 K. In addition to the family of Ru_2[II,III] complexes, tetra-amidinate-bridged Ru_2[III,III] complex Ru_2(4-I-bam)$_4Cl_2$ (4-I-bam = 4-iodobenzamidinate) was prepared by analogous synthetic chemistry.

The formation of Ru–Cl–Ru chains in the solid-state structures of Ru_2L_4Cl complexes typically leads to poor solubility in many organic solvents (see for example the structure of

Ru_2(4-I-HNBz)$_4$Cl, Figure S1 and Table S1). To increase the solubility of these complexes, we replaced the axially bound chloride ligand with tetrafluoroborate by treatment with silver tetrafluoroborate. The anion exchange process was monitored by IR spectroscopy, which showed the characteristic broad B–F stretch of BF_4^- at 1050 cm^{-1} (Figure S4), and elemental analysis. Single crystal X-ray diffraction analysis of $Ru_2(HNBz)_4BF_4$ (Figure S5 and Table S2) reveals the two axial positions of the Ru_2 unit are occupied by a water and a THF ligand, respectively. The electronic absorption spectra and ^1H NMR spectra of the tetrafluoroborate complexes are similar to those of the related chloride complexes (Figures S2, S6, and S7).

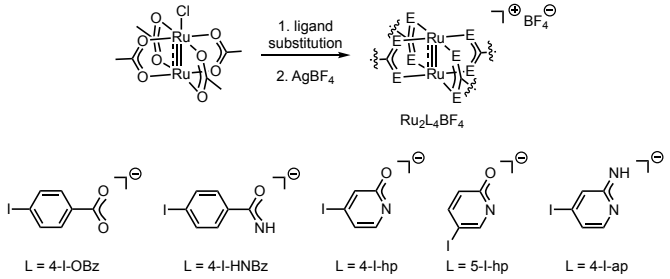

Figure 2. Five $Ru_2L_4BF_4$ complexes were prepared by a two-step procedure of ligand substitution and anion exchange. These complexes feature carboxylate (L = 4-I-OBz), amidate (L = 4-I-HNBz), 2-oxypyridinate (L = 4-I-hp or 5-I-hp), and 2-aminopyridinate (L = 4-I-ap) as the primary coordination spheres, respectively.

Table 1. The Ru_2-based polymeric materials were synthesized from Sonogashira cross-coupling reaction between Ru_2 molecular complexes and alkyne-based linkers of **A**, **B**, and **C**. The surface areas of these materials were probed by N_2 adsorption isotherm at 77 K. BET (Langmuir) surface area values (m^2/g) are listed as below for the obtained polymeric materials.

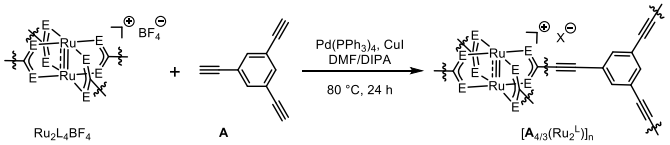

BET (Langmuir) / m^2/g	Ru_2(4-I-OBz)$_4BF_4$	Ru_2(4-I-HNBz)$_4BF_4$	Ru_2(4-I-hp)$_4BF_4$	Ru_2(5-I-hp)$_4BF_4$	Ru_2(4-I-ap)$_4BF_4$
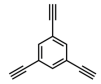 **A**	$[\mathbf{A}_{4/3}(Ru_2^{OBz})]_n$ Nonporous	--	$[\mathbf{A}_{4/3}(Ru_2^{4\text{-hp}})]_n$ 499 (782)	$[\mathbf{A}_{4/3}(Ru_2^{5\text{-hp}})]_n$ 329 (516)	--
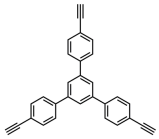 **B**	$[\mathbf{B}_{4/3}(Ru_2^{OBz})]_n$ 392 (616)	$[\mathbf{B}_{4/3}(Ru_2^{HNBz})]_n$ 260 (409)	$[\mathbf{B}_{4/3}(Ru_2^{4\text{-hp}})]_n$ 644 ± 11 (1012 ± 18)	$[\mathbf{B}_{4/3}(Ru_2^{5\text{-hp}})]_n$ 575 (902)	$[\mathbf{B}_{4/3}(Ru_2^{ap})]_n$ 457 (718)
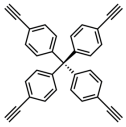 **C**	$[\mathbf{C}(Ru_2^{OBz})]_n$ 353 (554)	$[\mathbf{C}(Ru_2^{HNBz})]_n$ 491 (773)	$[\mathbf{C}(Ru_2^{4\text{-hp}})]_n$ 601 (943)	$[\mathbf{C}(Ru_2^{5\text{-hp}})]_n$ 696 (1093)	--

Synthesis of Ru_2-based polymers. A mixture of $Ru_2(4\text{-I-hp})_4BF_4$ and 1,3,5-triethynylbenzene (**A**) in 1 : 1 *N,N*-dimethylformamide (DMF) and diisopropylamine (DIPA) was heated at 80 °C for 24 hours under an N_2 atmosphere (Table 1 and details in Table S3). The harvested orange material, *i.e.* $[\mathbf{A}_{4/3}(Ru_2^{4\text{-hp}})]_n$, did not dissolve in any common solvents, such as dimethyl sulfoxide (DMSO), methanol (MeOH), and tetrahydrofuran (THF). Soxhlet extraction using MeOH was carried out to ensure complete removal of any unincorporated monomer units. The obtained solid did not display an IR feature of alkyne C–H stretching at 3288 cm^{-1} (Figure S8a) and showed trace amount of iodine from elemental analysis, consistent with a high degree of polymerization via Sonogashira cross coupling.

The developed polymerization chemistry is modular; both the polyalkyne and the Ru_2 monomer can be easily replaced by different reaction partners. In addition to *tris*-alkyne **A**, we have carried out polymerization reactions with 1,3,5-tris(4-ethynylphenyl)benzene (**B**), an extended version of **A**, and tetra(4-ethnylphenyl)methane (**C**), which features a tetrahedrally disposed array of terminal alkynes (Table 1). In addition to polymerization with $Ru_2(4\text{-I-hp})_4BF_4$, we have carried out metallopolymerization reactions with each of the iodinated Ru_2 complexes described above. Polymerization of $Ru_2(4\text{-I-bam})_4Cl_2$ with tris-alkyne **B** provided access to $[\mathbf{B}_{4/3}(Ru_2^{bam})]_n$. In each case, insoluble materials were obtained and IR analysis (Figure S8) indicated a high degree of polymerization.

Based on powder X-ray diffraction (PXRD) analysis, all of the prepared materials are amorphous (PXRD data for the five polymers prepared from linker **B** are collected in Figure S9), which is consistent with previous reports that Sonogashira cross-coupling reactions provide access to amorphous POPs.[27, 35] Thermogravimetric analysis (TGA) revealed this family of materials is thermally stable to above 200 °C (Figure S10). For example, $[\mathbf{B}_{4/3}(Ru_2^{4\text{-hp}})]_n$ is stable up to 250 °C after which temperature continuous weight loss is observed (Figure S10c).

Gas sorption. N_2 adsorption isotherms were collected at 77 K for each of the Ru_2-based polymers in order to evaluate the porosity of these materials; data is collected in Table 1, Figure S11, and Figure S12. Each material was pre-activated at 150 °C under reduced pressure (<10 μbar) for 16 h. With the exception of $[\mathbf{A}_{4/3}(Ru_2^{OBz})]$, each of the polymers reported here displays permanent porosity, with Brunauer–Emmett–Teller (BET) surface areas from 260 – 696 m^2/g. These surface areas are similar to those reported with POPs derived from Sonogashira reactions.[35]

Both synthetic conditions utilized to prepare the polymeric materials and activation protocol are important to achieving high surface areas. Initial attempts towards $[\mathbf{A}_{4/3}(Ru_2^{5\text{-hp}})]_n$ utilized $Ru_2(5\text{-I-hp})_4Cl$, which is poorly soluble in the reaction medium, as the metallomonomor. The resulting material was found to be non-porous. In contrast, polymerization of the more soluble tetrafluoroborate complex $Ru_2(5\text{-I-hp})_4BF_4$ provided $[\mathbf{A}_{4/3}(Ru_2^{5\text{-hp}})]_n$, which displayed a BET surface area of 329 m^2/g (Langmuir surface area of 526 m^2/g). With respect to activation, Soxhlet extraction with MeOH was found to be critical. For example, comparison of the N_2 uptake of a sample of $[\mathbf{A}_{4/3}(Ru_2^{4\text{-hp}})]_n$ obtained directly from synthesis to that of $[\mathbf{A}_{4/3}(Ru_2^{4\text{-hp}})]_n$ extracted by MeOH for 48 h is shown in Figure S11g. A significant increase of N_2 uptake capacity was observed from 114 cm^3/g (P/P_0 = 0.3) of the unextracted sample to 175 cm^3/g (P/P_0 = 0.3) of the extracted sample,

which corresponds to BET surface areas of 389 m^2/g (Langmuir surface area at 462 m^2/g) and 499 m^2/g (Langmuir surface area at 782 m^2/g), respectively.

For a given Ru_2 unit, increasing the alkyne linker length (from **A** to **B**) or moving from *tris*-alkyne **A** to *tetra*-alkyne **C** enhanced the surface area of the resulting polymer. For example, in the case of $Ru_2(4\text{-I-OBz})_4BF_4$, $[\mathbf{B}_{4/3}(Ru_2^{OBz})]_n$ and $[\mathbf{C}(Ru_2^{OBz})]_n$ exhibited BET surface areas of 392 and 352 m^2/g, respectively, while $[\mathbf{A}_{4/3}(Ru_2^{OBz})]_n$ was determined to be nonporous. A similar trend was observed with metallopolymers based on both $Ru_2(4\text{-I-hp})_4BF_4$ and $Ru_2(5\text{-I-hp})_4BF_4$ (Table 1). To evaluate the reproducibility of the described synthetic method, three batches of $[\mathbf{B}_{4/3}(Ru_2^{4\text{-hp}})]_n$ were prepared from independent reactions and were characterized by gas sorption (Figure S11d). The BET surface areas determined for these samples were 641 m^2/g, 627 m^2/g, and 666 m^2/g, respectively, with the average value of 644 ± 11 m^2/g, which validated the reproducibility of the synthetic protocol.

X-ray absorption spectroscopy. To interrogate the valence and the local coordination geometry of the Ru sites embedded in these amorphous porous materials, we have pursued X-ray absorption spectroscopy (XAS) experiments. For reference, we have also collected XAS data for the iodinated molecular Ru_2 complexes prior to polymerization. X-ray absorption near edge structure (XANES) provides a sensitive probe of the oxidation state of Ru_2 complexes,[31, 36] and collected data suggests that the Ru_2 units in materials of $[\mathbf{C}(Ru_2^{OBz})]_n$, $[\mathbf{C}(Ru_2^{HNBz})]_n$, $[\mathbf{C}(Ru_2^{4\text{-hp}})]_n$, and $[\mathbf{C}(Ru_2^{5\text{-hp}})]_n$ retain the Ru_2[II,III] structure of the molecular precursors (Figure S13). Extended X-ray fine structure (EXAFS) EXAFS data collected for this family of materials indicates that the local coordination geometry of polymerized Ru_2 sites is unchanged as compared with the relevant molecular precursors (data and analyses are collected in Figure S14 and Table S4). For example, the EXAFS data (Ru K-edge, Table S4) collected for $[\mathbf{C}(Ru_2^{HNBz})]_n$ indicates the presence of a pentacoordinate Ru environment comprised of two Ru–N distances at 1.99(1) Å, two Ru–O distance at 2.07(1) Å, and one Ru–Ru distance at 2.32(1) Å, which is consistent with the molecular structure of $Ru_2(HNBz)_4BF_4$ determined by single-crystal X-ray diffraction and EXAFS analysis.

Electronic structure. Evans method measurement of $Ru_2(4\text{-I-OBz})_4BF_4$ reveals its magnetic moment as 4.06 μ_B, which corresponds to three unpaired electrons.[37] This result is consistent with a quartet ground-state electronic configuration (*i.e.* $\sigma^2\pi^4\delta^2(\pi^*\delta^*)^3$) owing to the near degeneracy of the π^* and δ^* orbitals. This electronic configuration has been reported for $[Ru_2L_4]^+$ complexes with L = OBz, HNBz, hp, and ap in which the ligands are not iodinated.[38, 39] $Ru_2(4\text{-I-bam})_4Cl_2$ exhibits a triplet ground state (S = 1; electronic configuration of $\sigma^2\pi^4\delta^2\pi^{*2}$).[40]

The electronic absorption spectra of Ru_2 complexes has been the subject of extensive investigations.[38] The near IR (NIR) region of these spectra frequently contains absorbances attributable to $\delta(Ru_2) \rightarrow \delta^*(Ru_2)$ transitions. Experimentally, a weak NIR band (1136 nm for $Ru_2(4\text{-I-OBz})_4Cl$, 990 nm for $Ru_2(4\text{-I-HNBz})_4Cl$, 980 nm for $Ru_2(4\text{-I-ap})_4Cl$, 960 nm for $Ru_2(4\text{-I-hp})_4Cl$, 880 nm for $Ru_2(5\text{-I-hp})_4Cl$) is observed (Figures 3a), which is assigned as the transition of $\delta(Ru_2) \rightarrow \delta^*(Ru_2)$. The spectra of $Ru_2(OAc)_4Cl$ (1133 nm) and $Ru_2(4\text{-I-OBz})_4Cl$ (1136 nm) display vibronic *x,y*-polarized component of the $\delta \rightarrow \delta^*$ transition (based on a 1450 cm^{-1} ν(COO) vibration), instead of two electronic excited states.[41-43] When

changing the primary coordination sphere from *O,O*-donor carboxylate (L = 4-I-OBz) to *N,O*- or *N,N*-donor ligands (L = 4-I-HNBz, 4-I-hp, 5-I-hp, and 4-I-ap), the $\delta \rightarrow \delta^*$ transition energy increases which manifests as a blue-shift of the NIR peaks. In these molecular complexes, the peak between 464 – 528 nm has been assigned as as π (Ru–E, Ru_2) → $\pi^*(Ru_2)$.[38] $Ru_2(4\text{-I-bam})_4Cl_2$ does not display any NIR absorption features.

To evaluate the relationship between the electronic structures of Ru_2 metallomonomers and polymer-confined Ru_2 sites, diffuse-reflectance UV-vis-NIR spectra were collected on the family of Ru_2-based polymers prepared from *tris*-alkyne **B** (Figures 3b). The collected spectra of the polymeric materials all display a strong absorption peak centered at 275 nm due to ligand-based $\pi \rightarrow \pi^*$ transitions. Relatively weak NIR absorbances are observed for each polymer material: $[\mathbf{B}_{4/3}(Ru_2^{4\text{-hp}})]_n$ (1035 nm), $[\mathbf{B}_{4/3}(Ru_2^{HNBz})]_n$ (980 nm), and $[\mathbf{B}_{4/3}(Ru_2^{ap})]_n$ (945 nm). The broadness of the NIR absorbances of $[\mathbf{B}_{4/3}(Ru_2^{OBz})]_n$ and $[\mathbf{B}_{4/3}(Ru_2^{5\text{-hp}})]_n$ prevent absolute assignment of the absorbance maxima of these materials, however, based on the peaks shapes of these materials and the absorbances determined for $[\mathbf{B}_{4/3}(Ru_2^{4\text{-hp}})]_n$, $[\mathbf{B}_{4/3}(Ru_2^{HNBz})]_n$, and $[\mathbf{B}_{4/3}(Ru_2^{ap})]_n$, the energies of the NIR absorbances of these materials appear to mirror the relative ligand-dependent energies observed in the metallomonomores.

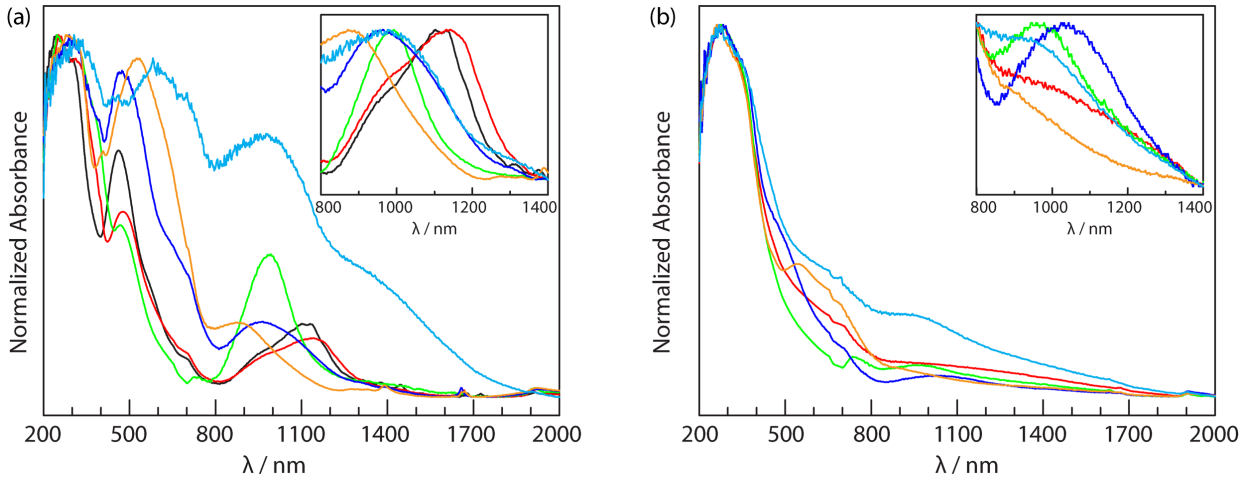

Figure 3. (a) Diffuse-reflectance UV-vis-NIR spectra were collected on the molecular complexes of $Ru_2(OAc)_4Cl$ (—), $Ru_2(4\text{-I-OBz})_4Cl$ (—), $Ru_2(4\text{-I-HNBz})_4Cl$ (—), $Ru_2(4\text{-I-hp})_4Cl$ (—), $Ru_2(4\text{-I-HNBz})_4Cl$ (—), and $Ru_2(4\text{-I-ap})_4Cl$ (—). (b) Diffuse-reflectance UV-vis-NIR spectra were collected on the polymeric materials of $[\mathbf{B}_{4/3}(Ru_2^{OBz})]_n$ (—), $[\mathbf{B}_{4/3}(Ru_2^{HNBz})]_n$ (—), $[\mathbf{B}_{4/3}(Ru_2^{4\text{-hp}})]_n$ (—), $[\mathbf{B}_{4/3}(Ru_2^{5\text{-hp}})]_n$ (—), and $[\mathbf{B}_{4/3}(Ru_2^{ap})]_n$ (—). The absorbance spectra were normalized to the highest peaks between 200 and 300 nm. The insert spectra were normalized to the highest peaks between 800 and 1400 nm.

Amination catalysis. *Intramolecular C–H amination.* Molecular Ru_2[II,III] catalysts have previously been applied to nitrene-transfer catalysis using iminoiodinane reagents as nitrene sources.[44] As illustrated in Table 2, the reactive Ru_2 nitrenoids invoked as intermediates in these reactions can participate in both allylic amination (*i.e.* conversion of **1** to **2**) and olefin aziridination (*i.e.* conversion of **1** to **3**). Du Bois and co-workers have demonstrated that the primary coordination sphere of Ru_2 has a profound impact on the

selectivity of nitrene transfer chemistry: When $Ru_2(OAc)_4Cl$ is used as the catalyst for intramolecular nitrene transfer in **1**, a 1:3 ratio of **2** and **3** are obtained; when $Ru_2(hp)_4Cl$ is used as the ligand for a Ru_2 catalyst, an 8:1 ratio of **2** and **3** are obtained.[44]

Each of the molecular Ru_2[II,III] metallomonomers utilized in this study is a competent catalyst for intramolecular nitrene transfer. The catalyst-dependent product ratios (**2** vs. **3**) are reported in Table 2 and confirm the impact of the primary coordination sphere on the selectivity for allylic amination versus olefin aziridination. We have evaluated our family of porous Ru_2[II,III] polymers for intramolecular nitrene transfer with olefinic substrate **1** in order to evaluate the impact of primary coordination sphere of polymer-supported Ru_2 sites on nitrene-transfer chemoselectivity. Each of the polymers developed here is a competent catalyst for the illustrated nitrene transfer reaction (details in Table S5). The reactions catalysed by 3.7 mol% molecular complexes completed in 16 h according to the disappearance of $PhI(OAc)_2$ from ^1H NMR. The reaction catalysed by polymeric materials were loaded with 10.0 mol% and extended from 16 h to 24 h. The ratio of **2**:**3** were observed to be independent from the reaction time. The sequence of **2** : **3** ratio from the polymeric materials displays as $[\mathbf{B}_{4/3}(Ru_2^{4\text{-hp}})]_n$ > $[\mathbf{B}_{4/3}(Ru_2^{5\text{-hp}})]_n$ ≈ $[\mathbf{B}_{4/3}(Ru_2^{ap})]_n$ > $[\mathbf{B}_{4/3}(Ru_2^{HNBz})]_n$ > $[\mathbf{B}_{4/3}(Ru_2^{OBz})]_n$ (Entry 6 to Entry 10, Table 2). The observed sequence of product ratio from homogeneous molecular catalysts is $Ru_2(4\text{-I-hp})_4BF_4$ > $Ru_2(4\text{-I-ap})_4BF_4$ > $Ru_2(5\text{-I-hp})_4BF_4$ > $Ru_2(4\text{-I-HNBz})_4BF_4$ > $Ru_2(4\text{-I-OBz})_4BF_4$ (Entry 1 to Entry 5, Table 2). These data demonstrate that the ligand-dependent chemoselectivity observed with soluble molecular catalysts has been translated to the solid state. The similarity of the selectivity trends between molecular and polymer catalysts indicates that chemoselectivity derives primarily from the electronic structure of the catalyst and is not substantially impacted by confinement of the substrate within the porous catalyst material. [45]

Table 2. Intramolecular amination reaction catalysed by molecular complexes and Ru_2-based polymeric materials.[a]

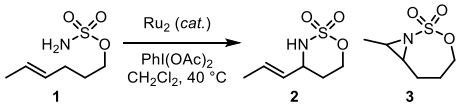

1 2 3

Entry	Catalyst	2:3	Entry	Catalyst	2:3
1	$Ru_2(4\text{-I-OBz})_4BF_4$	0.7:1	6	$[\mathbf{B}_{4/3}(Ru_2^{OBz})]_n$	1.1:1[b]
2	$Ru_2(4\text{-I-HNBz})_4BF_4$	1.4:1	7	$[\mathbf{B}_{4/3}(Ru_2^{HNBz})]_n$	1.3:1
3	$Ru_2(4\text{-I-hp})_4BF_4$	9.3:1	8	$[\mathbf{B}_{4/3}(Ru_2^{4\text{-hp}})]_n$	4.3:1
4	$Ru_2(5\text{-I-hp})_4BF_4$	2.0:1	9	$[\mathbf{B}_{4/3}(Ru_2^{5\text{-hp}})]_n$	3.2:1
5	$Ru_2(4\text{-I-ap})_4BF_4$	4.6:1	10	$[\mathbf{B}_{4/3}(Ru_2^{ap})]_n$	3.1:1

[a] Reactions were typically performed at 40 °C using 1.4 equiv. $PhI(OAc)_2$ with 3.7 mol% molecular Ru_2 complexes for 16 h or 10.0 mol% Ru_2-based polymeric catalysts for 24 h. Product ratios was calculated by integrals of GC spectra. [b] The data was collected with 30.0 mol% loading of $[\mathbf{B}_{4/3}(Ru_2^{OBz}]]_n$, given that the reaction catalysed by 10.0 mol% loading only provided <2 % of conversion.

Discussion The functionalization of C–H bonds by reactive M–L multiply bonded intermediates proceeds on a mechanistic continuum between concerted asynchronous insertion[46, 47] and stepwise radical abstraction / radical recombination chemistry.[48, 49] Controlling the electronic structure of the relevant reactive intermediates can provide a tool to influence the chemoselectivity of group transfer reactions. In the specific context of

nitrene-transfer catalysis, substantial progress has been achieved in controlling the chemoselectivity of nitrene transfer chemistry by tuning the primary ligand sphere of transition metal catalysts. MOFs have been advanced as a tool to address some of the pressing synthetic challenges in C–H amination chemistry — for example, realization of general platforms for selective intermolecular C–H amination — in that they provide a platform to non-covalently co-localize substrate in proximity to reactive intermediates. MOFs are often envisioned as platforms to heterogenize molecular catalysts – the coordination sphere of lattice-confined metal sites is well-defined, fairly uniform structurally, and easily characterized – however systematic variation of the primary ligand sphere of lattice-bound metal ions is in many cases not possible. In order to enable systematic investigation of potential porous catalysts as a function of the transition metal ligands, we have endeavored to develop synthetic tools to provide access to families of porous materials with site-isolated catalysts in which the donor atoms that support the transition metal sites could be systematically tuned.

We recognized that the challenge in accessing broad ligand families is due to the reliance on retrosynthetic disconnection of the M–L bonds in typical syntheses of these materials: The methods that are regularly employed to generate crystalline porous MOFs rely of reversible M–L bond-forming chemical reactions. The resulting lattice-confined transition metal sites are largely supported by weak-field ligands that engender high-spin electronic configurations. A fundamental challenge in utilizing MOF scaffolds as platforms to accomplish chemoselective group-transfer catalysis is developing synthetic chemistry that allows the atomistic control over the primary ligand sphere that is characteristic of molecular catalysis.

To circumvent the challenge of generating porous materials that are based on strongly basic ligands, which do not readily participate in reversible M–L bond formation, we have developed a synthetic approach predicated on retrosynthetic disconnection of covalent bonds in the organic linker. Here, we demonstrate that Sonogashira cross-coupling of metallomonomers with polyalkynes provides access to families of porous materials. The extent of polymerization is high (established by IR spectroscopy) and the resulting materials are permanently porous (established by N_2 uptake experiments). XAS measurements confirm that the valence (by XANES) and local coordination geometry (by EXAFS) are maintained during polymerization. This family of materials features identical structural elements but vary in the donor atom presented to the Ru_2 complexes that are housed within the porous architectures. Because the same bond disconnection is utilized to prepare the entire family of porous materials, a single set of reaction conditions provide ready access to a family of materials.

Each of the porous Ru_2[II,III]-based materials that we have prepared is competent as a nitrene-transfer catalyst. When challenged with a substrate that presents the possibility to undergo either allylic C–H amination or olefin aziridination, the chemoselectivity of the polymer-catalyzed nitrene transfer is sensitive to the primary coordination sphere of the Ru_2 site: increasingly strong donor ligands provide greater selectivity for allylic amination as compared with weaker donor ligands. The trends in chemoselectivity observed for the porous polymer materials mirrors that observed with molecular catalysts featuring an analogous set of supporting ligands. This set of experiments demonstrates that the

developed Sonogashira coupling strategy for polymerization of metallomonomers provides a platform to translate the chemoselectivity of molecular catalysts to porous materials platforms. Preliminary experiments have confirmed that intermolecular C–H amination is possible in the developed materials.

Conclusions

Based on the modular synthetic methods that underlie the burgeoning field of MOF chemistry, these materials have been advanced as platforms to rationally heterogenize available homogeneous catalysts. In this context, a large set of reactions have been demonstrated using available porous catalyst materials. In contrast to soluble molecular catalysts, synthetic limitations that are intrinsic to the synthesis of crystalline MOFs – namely the requirement that M–L bond-forming chemistry be reversible – prevent access to broad classes of potential catalyst materials in which the primary ligand sphere is comprised of donors that do not participate in reversible M–L bonding. Here, we demonstrate that atomistic control of the primary ligand sphere of lattice-confined catalysts can be achieved by polymerization of pre-formed metallomonomers. The resulting amorphous, permanently porous materials are competent catalysts for nitrene-transfer chemistry, and display ligand-dependent chemoselectivity that is analogous to homogenous counterparts. We anticipate that the developed polymerization strategy will expand the suite of porous catalyst materials that can be evaluated and provide additional opportunities to achieve chemoselective C–H functionalization chemistry in intermolecular contexts.

ACKNOWLEDGMENT

We thank Texas A&M University, the Welch Foundation (A-1907), and the U.S. Department of Energy (DE-SC0018977) for financial support. We thank Hong-Cai Zhou for use of a gas sorption equipment, François Gabbaï for use of an IR spectrometer, and Abraham Clearfield for use of a TGA. XAS data were collected at Sector 10, MRCAT, of the Advanced Photon Source at Argonne National Laboratory. MRCAT operations are supported by the Department of Energy and the MRCAT member institutions. This research used resources of the Advanced Photon Source, a U.S. Department of Energy (DOE) Office of Science User Facility operated for the DOE Office of Science by Argonne National Laboratory under Contract No. DE-AC02-06CH11357.

Correspondence

david.powers@chem.tamu.edu

References

1. W. Lu, Z. Wei, Z.-Y. Gu, T.-F. Liu, J. Park, J. Park, J. Tian, M. Zhang, Q. Zhang, T. Gentle III, M. Bosch and H.-C. Zhou, *Chem. Soc. Rev.*, 2014, **43**, 5561.

2. N. R. Catarineu, A. Schoedel, P. Urban, M. B. Morla, C. A. Trickett and O. M. Yaghi, *J. Am. Chem. Soc.*, 2016, **138**, 10826.

3. N. Masciocchi, S. Galli, G. Tagliabue, A. Sironi, O. Castillo, A. Luque, G. Beobide, W. Wang, M. A. Romero, E. Barea and J. A. R. Navarro, *Inorg. Chem.*, 2009, **48**, 3087.

4. K. C. Bentz and S. M. Cohen, *Angew. Chem., Int. Ed.*, 2018, DOI: 10.1002/anie.201806912.

5. S. G. Dunning, G. Nandra, A. D. Conn, W. Chai, R. E. Sikma, J. S. Lee, P. Kunal, J. E. Reynolds III, J.-S. Chang, A. Steiner, G. Henkelman and S. M. Humphrey, *Angew. Chem., Int. Ed.*, 2018, **57**, 9295.

6. J. He, N. W. Waggoner, S. G. Dunning, A. Steiner, V. M. Lynch and S. M. Humphrey, *Angew. Chem., Int. Ed.*, 2016, **55**, 12351.

7. R. E. Sikma, P. Kunal, S. G. Dunning, J. E. Reynolds III, J. S. Lee, J.-S. Chang and S. M. Humphrey, *J. Am. Chem. Soc.*, 2018, **140**, 9806.

8. S. Das, P. Heasman, T. Ben and S. Qiu, *Chem. Rev.*, 2017, **117**, 1515.

9. A. G. Slater and A. I. Cooper, *Science*, 2015, **348**, aaa8075.

10. C. S. Diercks and O. M. Yaghi, *Science*, 2017, **355**, eaal1585.

11. S.-Y. Ding and W. Wang, *Chem. Soc. Rev.*, 2013, **42**, 548.

12. N. Huang, P. Wang and D. Jiang, *Nat. Rev. Mater.*, 2016, **1**, 16068.

13. N. Chaoui, M. Trunk, R. Dawson, J. Schmidt and A. Thomas, *Chem. Soc. Rev.*, 2017, **46**, 3302.

14. Q. Sun, Z. Dai, X. Meng and F.-S. Xiao, *Chem. Soc. Rev.*, 2015, **44**, 6018.

15. Y. Xu, S. Jin, H. Xu, A. Nagai and D. Jiang, *Chem. Soc. Rev.*, 2013, **42**, 8012.

16. P. Kaur, J. T. Hupp and S. T. Nguyen, *ACS Catalysis*, 2011, **1**, 819.

17. L. Zou, Y. Sun, S. Che, X. Yang, X. Wang, M. Bosch, Q. Wang, H. Li, M. Smith, S. Yuan, Z. Perry and H.-C. Zhou, *Adv. Mater.*, 2017, **29**, 1700229.

18. G. Zhang and M. Mastalerz, *Chem. Soc. Rev.*, 2014, **43**, 1934-1947.

19. T. Tozawa, J. T. Jones, S. I. Swamy, S. Jiang, D. J. Adams, S. Shakespeare, R. Clowes, D. Bradshaw, T. Hasell, S. Y. Chong, C. Tang, S. Thompson, J. Parker, A. Trewin, J. Bacsa, A. M. Z. Slawin, A. Steiner and A. I. Cooper, *Nat. Mater.*, 2009, **8**, 973.

20. A. P. Côté, A. I. Benin, N. W. Ockwig, M. O'Keeffe, A. J. Matzger and O. M. Yaghi, *Science*, 2005, **310**, 1166.

21. F. J. Uribe-Romo, J. R. Hunt, H. Furukawa, C. Klöck, M. O'Keeffe and O. M. Yaghi, *J. Am. Chem. Soc.*, 2009, **131**, 4570.

22. P. Kuhn, M. Antonietti and A. Thomas, *Angew. Chem., Int. Ed.*, 2008, **47**, 3450.

23. W. J. Ong and T. M. Swager, *Nat. Chem.*, 2018, **10**, 1023.

24. J.-X. Jiang, F. Su, A. Trewin, C. D. Wood, N. L. Campbell, H. Niu, C. Dickinson, A. Y. Ganin, M. J. Rosseinsky, Y. Z. Khimyak and A. I. Cooper, *Angew. Chem., Int. Ed.*, 2007, **46**, 8574.

25. O. K. Farha, A. M. Spokoyny, B. G. Hauser, Y.-S. Bae, S. E. Brown, R. Q. Snurr, C. A. Mirkin and J. T. Hupp, *Chem. Mater.*, 2009, **21**, 3033.

26. M. G. Schwab, B. Fassbender, H. W. Spiess, A. Thomas, X. Feng and K. Müllen, *J. Am. Chem. Soc.*, 2009, **131**, 7216.

27. J. R. Holst, E. Stöckel, D. J. Adams and A. I. Cooper, *Macromolecules*, 2010, **43**, 8531.

28. C. R. Wade and M. Dincă, *Dalton Trans*, 2012, **41**, 7931.

29. O. Kozachuk, K. Yusenko, H. Noei, Y. Wang, S. Walleck, T. Glaser and R. A. Fischer, *Chem. Commun.*, 2011, **47**, 8509.

30. A. Varela-Álvarez, T. Yang, H. Jennings, K. P. Kornecki, S. N. Macmillan, K. M. Lancaster, J. B. Mack, J. Du Bois, J. F. Berry and D. G. Musaev, *J. Am. Chem. Soc.*, 2016, **138**, 2327.

31. C.-H. Wang, A. Das, W.-Y. Gao and D. C. Powers, *Angew. Chem., Int. Ed.*, 2018, **57**, 3676.

32. D. J. Xiao, E. D. Bloch, J. A. Mason, W. L. Queen, M. R. Hudson, N. Planas, J. Borycz, A. L. Dzubak, P. Verma, K. Lee, F. Bonino, V. Crocellà, J. Yano, S. Bordiga, D. G. Truhlar, L. Gagliardi, C. M. Brown and J. R. Long, *Nat. Chem.*, 2014, **6**, 590.

33. L. Wang, D. W. Agnew, X. Yu, J. S. Figueroa and S. M. Cohen, *Angew. Chem., Int. Ed.*, 2018, **57**, 511-515.

34. B. Zhang, M. Wei, H. Mao, X. Pei, S. A. Alshmimri, J. A. Reimer and O. M. Yaghi, *J. Am. Chem. Soc.*, 2018, **140**, 12715.

35. J.-X. Jiang, F. Su, A. Trewin, C. D. Wood, H. Niu, J. T. A. Jones, Y. Z. Khimyak and A. I. Cooper, *J. Am. Chem. Soc.*, 2008, **130**, 7710.

36. W. Zhang, K. Freitag, S. Wannapaiboon, C. Schneider, K. Epp, G. Kieslich and R. A. Fischer, *Inorg. Chem.*, 2016, **55**, 12492.

37. R. J. H. Clark and M. L. Franks, *J. Chem. Soc., Dalton Trans.*, 1976, 1825.

38. M. A. S. Aquino, *Coord. Chem. Rev.*, 1998, **170**, 141.

39. M. C. Barral, S. Herrero, R. Jiménez-Aparicio, M. R. Torres and F. A. Urbanos, *Angew. Chem., Int. Ed.*, 2005, **44**, 305.

40. Y. Kataoka, S. Mikami, H. Sakiyama, M. Mitsumi, T. Kawamoto and M. Handa, *Polyhedron*, 2017, **136**, 87.

41. V. M. Miskowski and H. B. Gray, *Inorg. Chem.*, 1988, **27**, 2501.

42. V. M. Miskowski, T. M. Loehr and H. B. Gray, *Inorg. Chem.*, 1987, **26**, 1098.

43. C. R. Wilson and H. Taube, *Inorg. Chem.*, 1975, **14**, 2276.

44. M. E. Harvey, D. G. Musaev and J. Du Bois, *J. Am. Chem. Soc.*, 2011, **133**, 17207.

45. W.-Y. Gao, A. D. Cardenal, C.-H. Wang and D. C. Powers, *Chem. Eur. J.*, 2018, DOI: 10.1002/chem.201804490.

46. K. W. Fiori and J. Du Bois, *J. Am. Chem. Soc.*, 2007, **129**, 562.

47. H. M. L. Davies and J. R. Manning, *Nature*, 2008, **451**, 417.

48. B. Meunier, S. P. de Visser and S. Shaik, *Chem. Rev.*, 2004, **104**, 3947.

49. M. Newcomb and P. H. Toy, *Acc. Chem. Res.*, 2000, **33**, 449.